THE Q U BOLOMETRIC INTERFEROMETER FOR COSMOLOGY (QUBIC)

ESA/ESTEC, NOORDWIJK, THE NETHERLANDS
6-9 OCTOBER 2015

Créidhe O'Sullivan [1], Stephen Scully [1], Donnacha Gayer[1], Marcin Gradziel[1], J. Anthony Murphy[1], Marco De Petris[2], Daniele Buzi [2], Massimo Gervasi[3], Mario Zannoni[3], Jean-Christophe Hamilton [4], Michel Piat [4], Marie-Anne Bigot-Sazy [4], Julien Brossard [4], Bruno Maffei [5] on behalf of the QUBIC Collaboration

[1] Dept. of Exp. Physics, National University of Ireland, Maynooth, Co. Kildare, Ireland, creidhe.osulivan@nuim.ie
[2] Dip. Fisica - Univ. di Roma "La Sapienza", Piazzale Aldo Moro 2, 00185 Roma, Italy, marco.depetris@roma1.infn.it
[3] Physics Dept. "G. Occhialini", University of Milano Bicocca, 20126 Milan, Italy, massimo.gervasi@mib.infn.it
[4] APC, Université Paris Diderot-Paris 7, 10 rue Alice Domon et Léonie Duquet, 75205 Paris, France, hamilton@apc.univ-paris7.fr
[5] School of Physics and Astronomy, The University of Manchester, Manchester M13 9PL, UK, bruno.maffei@manchester.ac.uk

ABSTRACT

QUBIC is a novel ground-based instrument that aims to detect the very faint B-mode polarisation pattern in the Cosmic Microwave Background. Since gravitational waves are the only way to produce this type of polarisation at large angular scales, B-modes are a key prediction of Inflation, the leading theory of the very early Universe. No confirmed primordial B-mode detection has ever been made.
QUBIC uses bolometric interferometry, a technique that can combine the sensitivity of an imager with the immunity to systematic effects of an interferometer. It will directly observe the sky through an array of entry horns whose signals will be superimposed using a quasi-optical beam combiner. Images of the resulting interference fringes will be formed on two focal planes tiled with TES bolometers.
This paper focuses on the design and modelling of the QUBIC beam combiner, including the feedhorn array, optics and shielding. The modelling was carried out using a combination of ray-tracing, a paraxial diffraction analysis and physical optics, with both commercial and in-house software.

1. INTRODUCTION

1.1. Primordial B-modes in the Cosmic Microwave Background

The Cosmic Microwave Background (CMB) is a background of thermal radiation left from an early hot dense phase of the Universe. As Universe expanded, it redshifted the radiation so that today its spectrum peaks at millimetre wavelengths. The CMB is almost, but not quite, isotropic as structure formation resulted in both temperature and polarisation anisotropies. Observations of the CMB and its features provide a sensitive test of theories of the early Universe and to-date all these observations are consistent with the Big Bang theory plus a brief period of extremely rapid expansion known as Inflation. One key prediction of the theory of Inflation is the existence of gravitational waves that give rise to extremely faint odd-parity polarisation patterns in the CMB known as B-modes. These are at a significantly lower level than even-parity E-mode polarisation left by structure formation. No measurement of primordial B-modes has ever been made.
The level of primordial B-modes depends strongly on the energy scale of Inflation and is usually described in terms of a parameter r, the tensor-to-scalar ratio, that compares the level of B-mode to E-mode polarisation. ESA's Planck mission has placed an upper bound on this ratio of $r_{0.002} < 0.11$ (95% CL) [1] and the simplest inflationary models predict $r > 0.1$.

1.2. QUBIC

The Q U Bolometric Interferometer for Cosmology (QUBIC) [2] is a ground-based experiment that will target large angular scales around the $l \approx 100$ recombination peak in the B-mode angular power spectrum. It aims to constrain the tensor-to-scalar ratio in the range $0.01 < r < 0.1$ by exploiting the sensitivity of bolometers combined with the control of systematic errors offered by interferometry. This bolometric interferometry technique was first demonstrated by the Millimeter-wave Bolometric Interefrometer [3]. The QUBIC collaboration formed from the merger of the MBI and BRAIN [4] projects in 2008 and is an international collaboration involving several universities and laboratories in France, Italy, the UK, the US, the Netherlands and Ireland.
The initial plan is that QUBIC be composed of 6 interferometer modules, two each operating at three different frequencies (97, 150 and 220 GHz) with 25% bandwidth. The first module will be at 150 GHz and comprise 400 back-to-back horns whose signals will be added using a quasi-optical combiner. The resulting interference fringes will be imaged on a cooled array of 1024 TES bolometers in order to achieve background-limited sensitivity. A rotating half-wave plate (HWP)

and polariser will be used to directly construct synthetic images of the I, Q and U Stokes parameters observed through the instrument primary beam. An autocalibration technique, making use of redundant baselines, has been developed [5,6] so that QUBIC will achieve unprecedented control of systematics along with a sensitivity comparable to that of more traditional imaging polarimeters. QUBIC will make observations at the Franco-Italian Concordia station in Dôme C, Antarctica. The first module is under construction and will begin observations there in late 2016. Simulations have shown that this first module (with a beam FWHM of 14°) could constrain the tensor-to-scalar ratio down to $r < 0.05$ after two years of observing.

1.3. Fizeau Interferometry

QUBIC operates as a Fizeau interferometer: the beams from an array of back-to-back horns at the entrance aperture are superimposed on a focal plane by the beam combiner. Each pair of horns produces a fringe pattern on this focal plane and, for perfect imaging, equivalent baselines produce identical fringe patterns. The fringe pattern image is sampled by an array of bolometers, hence the term *bolometric interferometry*. The complex fringe visibility could be measured from this image but QUBIC will be used as a synthetic imager, observing the fringes from all baselines simultaneously. The combined fringe pattern is simply an image of the sky convolved with the synthesised beam of the instrument. This synthesised beam is largely determined by the location of the horns in the input array (the maximum baseline determines its FWHM). The field-of-view is determined by their beam pattern.

2. DESIGN OF THE QUBIC BEAM COMBINER

QUBIC will observe at 150 GHz, in the first instance (see §5 for high-frequency extension), and sample the range of multipoles $l \approx 30$ - 200 in the sky. The combiner must be a focusing system so that beams from each of the re-emitting horns are superimposed on the focal plane (Fig. 1). The combiner is therefore an imager and, in the absence of aberrations, equivalent baselines (same length and direction) produce identical fringe patterns.

The practical limitation on the size and number of bolometers that could be produced for the focal plane, as well as the requirement to Nyquist sample the fringes from the largest multipoles, means that the focal length of the combiner is restricted to range of approximately 200 - 300 mm. The input array of 400 corrugated feedhorns has an aperture diameter of 300 mm (large, for sensitivity) meaning that this is a very fast optical system. The full combiner must fit into a cryostat of approximately 1 m^3.

The requirement that the telescope optics, particularly in terms of polarisation, should be accurately characterised favoured a reflecting rather than refracting design and an off-axis configuration was chosen in order to give a large unobstructed aperture. Aberrations were the main cause of concern for such a fast off-axis system but adding confocal subreflectors to a classical parabolic primary mirror gives the flexibility to cancel or reduce higher-order aberrations; space limitations restricted us to dual-reflector designs. It has been shown that any dual-reflector system consisting of offset confocal conic sections has an 'equivalent paraboloid' and that the relative tilt of the parent conic symmetry axes can be adjusted to make the equivalent paraboloid rotationally symmetric resulting in low cross-polarisation and low astigmatism [8,9]. This configuration, called a compensated system, is said to obey the Mizuguchi-Dragone condition. A classical compensated off-axis two-mirror telescope has zero linear astigmatism and coma (the dominant remaining aberration) identical to that of an on-axis paraboloidal mirror with the same focal ratio.

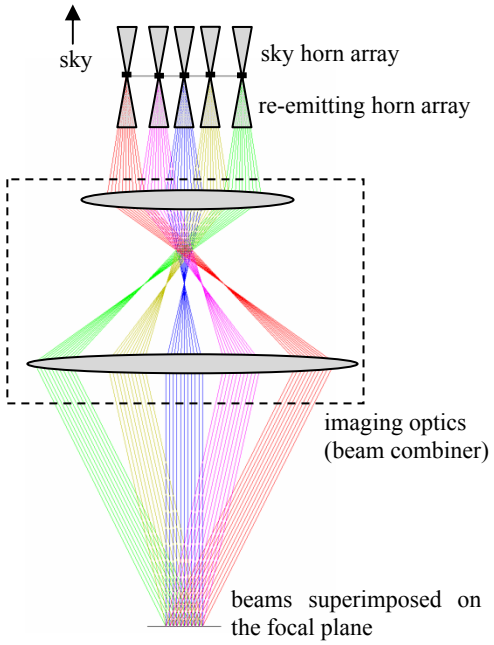

Figure 1. Schematic diagram of an idealised QUBIC instrument. It will observe the sky with a 22-element diameter array of back-to-back horn antennas . The beam combiner will superimpose the array of re-emitted beams on a focal plane. Here the beam combiner optics are represented by a pair of paraxial lenses. (The ray paths were generated using Zemax [7]).

We studied several designs for QUBIC [10] including compensated classical Cassegrain (parabolic primary, confocal hyperbolic secondary), Gregorian (parabolic primary, confocal elliptical secondary) and Dragonian (parabolic primary, confocal concave hyperbolic

secondary) dual reflectors. Both standard and crossed (front- and side-fed) geometries were considered. Side-fed crossed Dragone telescopes in particular have been shown to have large diffraction-limited field-of-view [11] but our short focal length and relatively large focal plane ruled out the crossed designs. A compensated off-axis Gregorian design was chosen that also obeyed the Rusch condition for minimum spillover [8]. A further optimisation of the mirror surfaces was carried out with the aid of commercial ray-tracing software (Zemax, [7]) to improve the diffraction-limited field-of-view (Fig. 2). The design is close to telecentric (distant exit pupil).

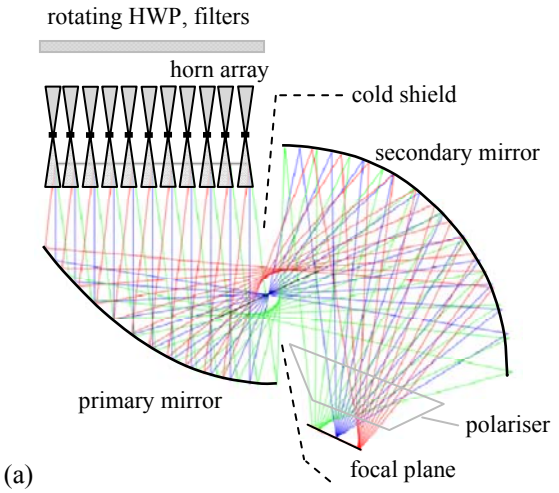

Figure 2. (a) The off-axis dual reflector chosen for the QUBIC beam combiner. The rays, at -7°, 0° and +7° represent the beams from the re-emitting horns. (b) Strehl ratio as a function of off-axis angle for the combiner in (a). A strehl ratio > 0.8 is considered essentially diffraction-limited. (The ray paths and strehl ratios were generated using Zemax [7].)

Two further elements needed to be added to the QUBIC combiner. Firstly, a polariser before the final focal plane in Fig. 2 will split the signal so orthogonal linear polarisations will be detected on separate focal planes and secondly a cold shield will be placed around the focal planes and secondary mirror to reduce background loading on the bare array of detector bolometers. A rotating half-wave plate [2] is also used.

3. OPTICAL SIMULATIONS

The final optimisation of the dual-reflector design was carried out using geometrical optics (ray-tracing) in order to take advantage of its speed and the optimisation routines available in commercial software packages. However, for a detailed analysis at these operating frequencies where component sizes are not very large compared with the wavelength of radiation, techniques that do not ignore the effects of diffraction must be used [12].
We start with the beams emitted by the downward facing horn array and propagate them through the optical system, primary then secondary mirror, and on to the focal plane. Initially we use a best-fit Gaussian beam as the horn beam and propagate it through an equivalent on-axis system using a Gaussian beam mode analysis and the ABCD technique (see [13]). This is a useful analysis for determining approximate beam sizes in the instrument and on the focal plane. Fig. 3(a) shows the QUBIC combiner's equivalent on-axis system and Fig. 3(b) shows the Gaussian beam radius as a function of propagation distance ($w(z)$) for a selection of re-emitting horn beam sizes. The initial waist radius is calculated as

$$w(0) = \sqrt{2\ln(2)}\,\frac{\lambda}{\pi\theta} \qquad (1)$$

where θ is the far-field divergence angle of the beam (FWHM of intensity in this case). Also shown is the is the total percentage of power from each beam that is captured by the QUBIC focal plane (radius r = 51 mm). For a 14° FWHM initial horn beam this is just over 74%.

For a more accurate determination of system performance and for the optimisation of the polariser and cold stop location, a full vector physical optics (PO) analysis of all 400 beams was carried out with our in-house software MODAL [14] and GRASP [15]. The beam emitted from the horns is calculated using a rigorous electromagnetic modematching technique [16] that views the corrugated structure as a sequence of smooth walled cylindrical waveguide sections each of which can support a set of TE and TM modes. At each corrugation there is a sudden change in the radius of the cylindrical guide and this change results in a scattering of power between the waveguide modes (the total power is conserved). In Fig. 4 an on-axis beam is plotted at a selection of planes as it propagates from the primary mirror to the focal plane. On the left, the beam (amplitude) calculated using PO is shown, and on the right the Gaussian

beam approximation as discussed previously. Fig. 4 illustrates that although a Gaussian beam mode analysis can be used to give a good estimate of beam size, PO should be used where the beams are aberrated. The compensating nature of the dual-reflector design is also clear.

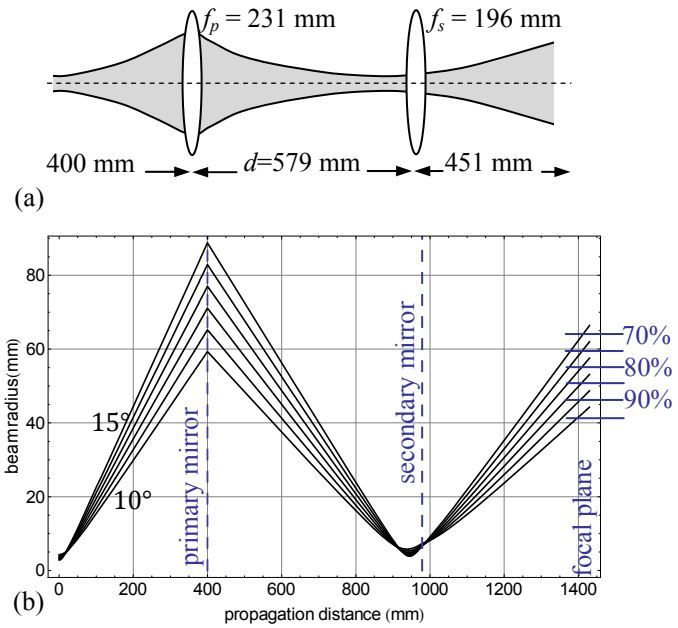

Figure 3. (a) Equivalent on-axis system for the beam combiner. The focal length of the system is given by

$$f_{eq} = \left(\frac{1}{f_p} + \frac{1}{f_s} - \frac{d}{f_p \times f_s}\right)^{-1} \approx 300 \text{ mm} .$$

(b) The Gaussian width as a function of propagation distance through the system for beams with varying far-field divergence angle. The power integrated by a 51-mm radius focal plane is also indicated.

Calculating the footprint of the beams at various planes in the system allowed the optimum size and location of components to be determined [17]. The example in Fig. 5 shows the footprint of the beams on the secondary mirror. A 14° FWHM Gaussian beam, propagated to our focal plane, has a radius of 62 mm and so will be captured down to an intensity level $I_0 \exp(-2(51/62)^2) \approx I_0 \exp(-2(0.8)^2)$, where I_0 is its peak intensity (this corresponds to approximately 72% of the power in the beam, as discussed for Fig. 3 before). For this reason we have coloured our footprint diagrams to show the region of each beam where the intensity is above $I_0 \exp(-2(0.8)^2)$; $\exp(-2(1)^2)$, $\exp(-2(2)^2)$ and $\exp(-2(3)^2)$ levels are also shown. The red-coloured region in Fig. 5, therefore, shows the area that must be covered by the mirror in order for at least 72% of the power from each of the 400 beams to be captured (this corresponds to much more than 72% of the total power, of course, since most beams are entirely covered).

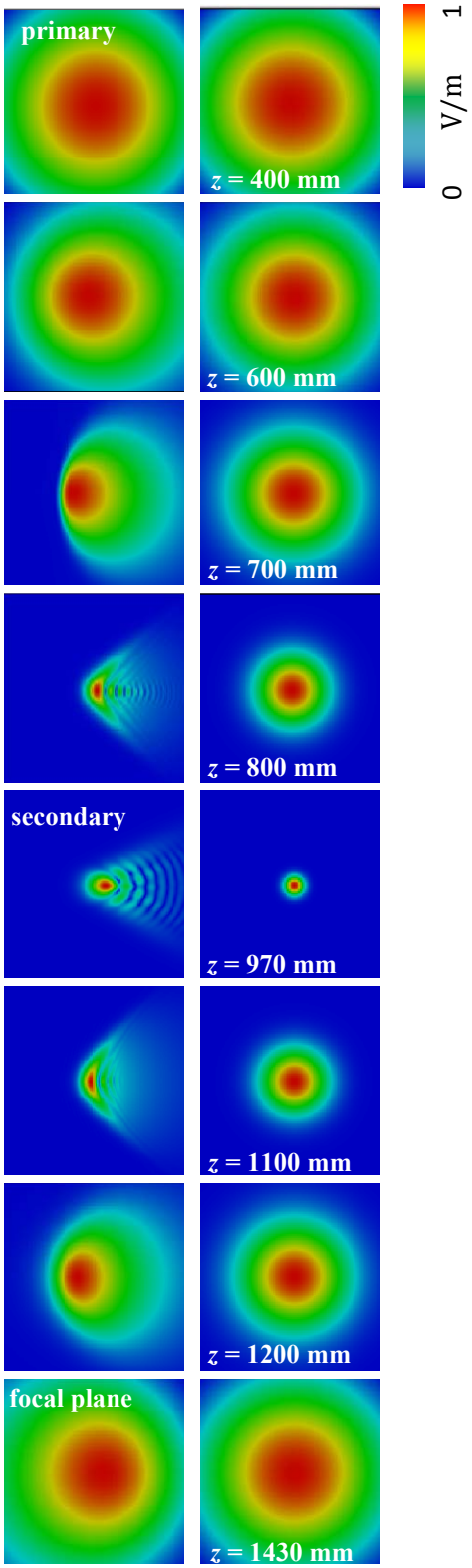

Figure 4. (Left) plots of the central horn beam (normalised amplitude) as it propagates from the primary mirror (z=0) to the focal plane and (right) the same beam as predicted using a single Gaussian beam and an ABCD analysis.

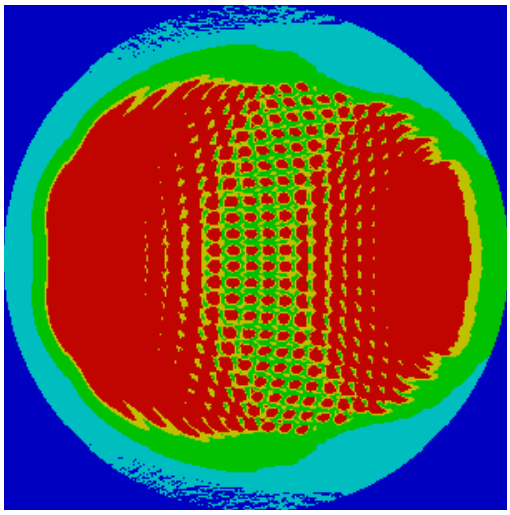

Figure 5. Footprint of 400 antenna beams on the 600-mm diameter secondary mirror. The regions coloured red show where the intensity of each beam is greater than $\exp(-2(0.8)^2)$ of its maximum. Yellow, green and light blue correspond to $\exp(-2(1)^2)$, $\exp(-2(2)^2)$ and $\exp(-2(3)^2)$, respectively [17].

This work was further developed [18] to fit a surface to the 'edge' of each of the beams in order to visualise their propagation through the optics (Fig. 6). The edge can be defined as the points at which the intensity drops to a certain level or, for complex beam shapes, the radius required to encircle a given percentage of power. The beams are first calculated at a series of planes in the system using PO. The beam edges are joined using interpolation and written to a `.stp` file so that they can be read into standard CAD software packages. In this way we can check for beam truncation by supporting structures, electronics etc.

Once all the component sizes and locations were chosen, the 400 antenna beams were propagated through the system to the focal plane. The focal plane for one configuration is shown in Fig. 7. The 400 plots of the focal plane beam are arranged so as to indicate the location of the horn antenna from which the beam originated. Here we can see the effect of reducing the size of the mirrors to $<$ 420 mm in each dimension (from 480×600 and 600×600 mm^2 for the primary and secondary, respectively). Plots such as these allowed us to quickly assess levels of aberration and truncation in our designs.

4. PERFORMANCE OF THE SYSTEM

4.1 Fringe patterns

In the initial versions of the QUBIC design the re-emitting horns had a FWHM of 14° and so we would like our imager to produce diffraction-limited images over this field-of-view. A ray tracing analysis showed that we could not achieve such a low level of aberration for all horns in the plane of asymmetry (Fig. 2(b)). In Fig. 8 we plot the fringe patterns generated by two orthogonal 27.5-λ baselines (the multipole corresponding to $b_\lambda = 27.5$ is given by $l = 2\pi b_\lambda \approx 173$). These baselines are along and perpendicular to the plane of symmetry of the combiner and so represent the best and worst-case in terms of aberrations, respectively. To illustrate the effect of such aberrations on the operation of the beam combiner we generated fringe patterns from a selection of 145 baselines ($b_\lambda = 50$ in this case). Fig. 9 shows the average pattern and also the standard deviation of intensity measurements on the focal plane. Because of aberrations, the fringe patterns are not identical, particularly at the edges of the focal plane, and so there is not complete constructive or destructive interference - the fringes become degraded. This means that the sensitivity of the interferometer to the corresponding angular scale will be reduced. We calculate the loss in sensitivity by considering the synthesised beam and resulting window function of the instrument [19,2] as outlined next.

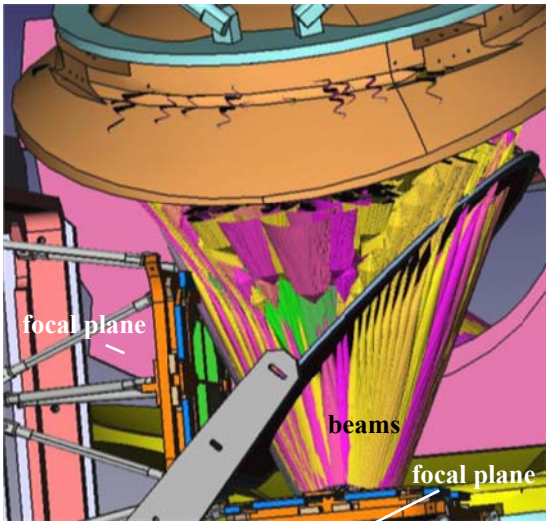

Figure 6. 3D rendering of the PO beams in a CAD model of the QUBIC combiner [18].

4.2 Window function

The instrument will make synthesised images of the sky $I, Q$and U Stokes parameters, and we can write this image (taking total intensity I as an example) as

$$S_I(p, \bar{n}_0, \theta_0) = \int I(\bar{n})\, B_s^p(\bar{n} - \bar{n}_0, \theta_0) d\bar{n} \qquad (2)$$

where $B_s^p(\bar{n}-\bar{n}_0,\theta_0)$ is the synthesised beam for the p^{th} bolometer in the focal plane when the telescope points in the direction $\bar{n}_0$ with pitch angle θ_0. As usual in CMB astronomy the sky intensity is decomposed into spherical harmonics

$$I(\bar{n}) = \sum_{lm} a_{lm} Y_{lm}^*(\bar{n}) \tag{3}$$

and for the CMB $\langle a_{lm} a_{l'm'}^* \rangle = C_l \delta_{ll'} \delta_{mm'}$. As described in [2], we introduce

$$\beta_{lm}(p,\bar{n}_0,\theta_0) = \int B_s^p(\bar{n}-\bar{n}_0,\theta_0)\, Y_{lm}(\bar{n}) d\bar{n} \tag{4}$$

so that the synthesised beam for the p^{th} bolometer can be written

$$B_s^p(\bar{n}-\bar{n}_0,\theta_0) = \sum_{lm} \beta_{lm}(p,\bar{n}_0,\theta_0) Y_{lm}\,, \tag{5}$$

and, making use of the orthogonality of the Y_{lm},

$$S_I(p,\bar{n}_0,\theta_0) = \sum_{lm} a_{lm} \beta_{lm}(p,\bar{n}_0,\theta_0)\,. \tag{6}$$

The covariance matrix of bolometer measurements

$$\begin{aligned} &\langle S_I(p,\bar{n}_k,\theta_i)\cdot S_I^*(q,\bar{n}_l,\theta_j)\rangle \\ &= \sum_{lm}\sum_{l'm'} a_{lm}\beta_{lm}(p,\bar{n}_k,\theta_i) a_{l'm'}^* \beta_{l'm'}^*(q,\bar{n}_l,\theta_j) \\ &= \sum_{l} C_l \sum_{m} \beta_{lm}(p,\bar{n}_k,\theta_i)\beta_{lm}^*(q,\bar{n}_l,\theta_j) \\ &= \sum_{l} C_l\, W_l(p,q,\bar{n}_k,\bar{n}_l,\theta_i,\theta_j) \end{aligned} \tag{7}$$

where we have introduced the window function

$$\begin{aligned} &W_l(p,q,\bar{n}_k,\bar{n}_l,\theta_i,\theta_j) \\ &= \sum_{m} \beta_{lm}(p,\bar{n}_k,\theta_i)\beta_{lm}^*(q,\bar{n}_l,\theta_j)\,. \end{aligned} \tag{8}$$

Similar window functions can be constructed for the other Stokes parameters and they give a measure of the sensitivity of the instrument to the different multipoles on the sky. Using our PO simulations to find B_s^p, we have calculated the diagonal window function for our aberrating beam combiner and compared it to that of an ideal one. The result, shown in Fig. 10, shows that the effect of the aberrations is to reduce the sensitivity of the instrument by 10%.

5. OPERATION AT 220 GHz

The doubt cast on the B-mode signal reported by the BICEP2 collaboration [20] by the Planck measurement of foreground dust polarisation has highlighted the importance of being able to make measurements at multiple frequencies in order to enable foreground separation. For this reason we decided to assess whether the first QUBIC module could operate as a dual-frequency instrument (150 and 220 GHz). In this case the polariser will moved in front of the sky-facing horns, after the HWP, and be replaced by a dichroic.

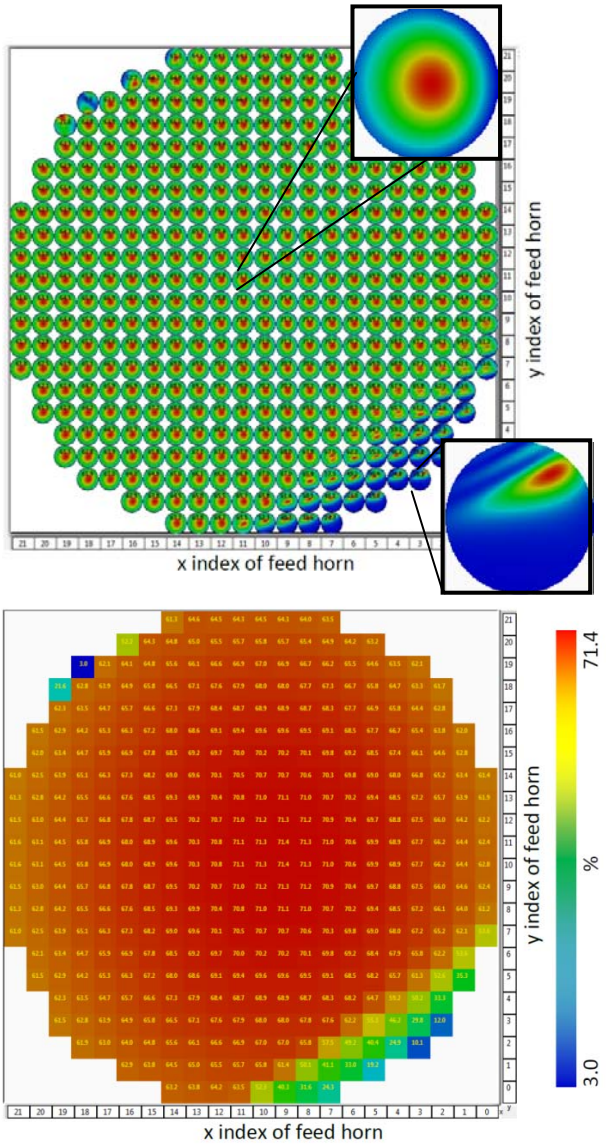

Figure 7. (a) Maps of the beam pattern from each of 400 input horns on the circular focal plane. The location of the input horn in the array is indicated by the placement of the focal plane plot. The total percentage of power from each beam that is integrated on the focal plane (limited to ~72% in this example by the finite size of the focal plane) is shown in (b).[17]

The design of the back-to-back horn antennas was changed from the original (scaled versions of the Clover [21] horns) so that they could operate over an extended range from 130 – 250 GHz. At the same time the beam was narrowed to 12.9°. As the operating frequency increases these horns allow

more hybrid modes to propagate, keeping the beam width approximately constant over the band (Fig. 11). Five modes can propagate at the high-frequency end of the band, the number that do propagate depends on how the sky signal couples to the input horns. We analysed the combiner design in the same way as before (optimising component sizes and locations) propagating each mode separately.

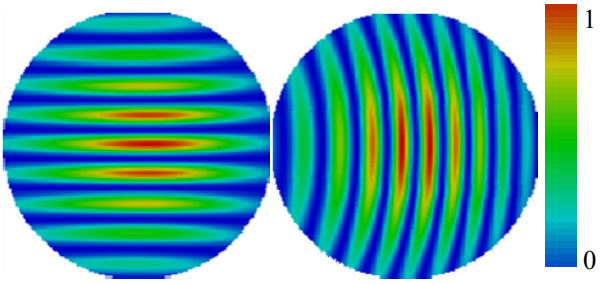

Figure 8. Fringe pattern generated on the r = 51 mm focal plane (intensity, arbitrary units).

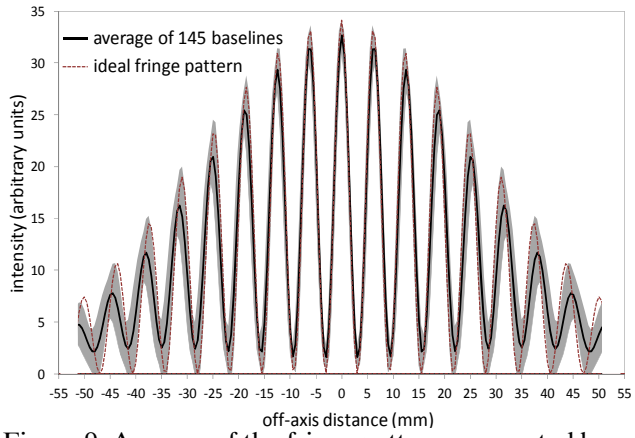

Figure 9. Average of the fringe patterns generated by 145 equivalent $b_\lambda = 50$ baselines. The standard deviation of the patterns is indicated by the grey shading and the dashed line shows the ideal fringe pattern.

Fig. 12 shows the point-spread-function (PSF) calculated by exciting the input horn array with an on-axis plane wave and summing the 400 focal plane patterns. On the left is the original 150-GHz PSF that corresponds to the window function in Fig. 10 and, on the right, the PSF of the dual-band instrument operating at 150 GHz. The location of the subsidiary peaks depends on the separation of horns in the aperture array and the width of the peaks depends on the number of horns. The amplitude is determined by the amplitude of the horn beam pattern on the focal plane. The slightly smaller beam of the new design improves the performance of the combiner.

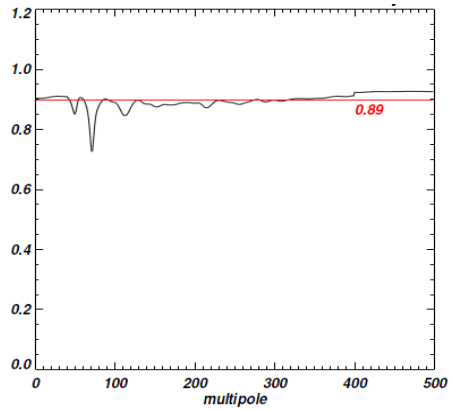

Figure 10. Diagonal window function of the real beam combiner divided by that of an ideal non-aberrating instrument [19].

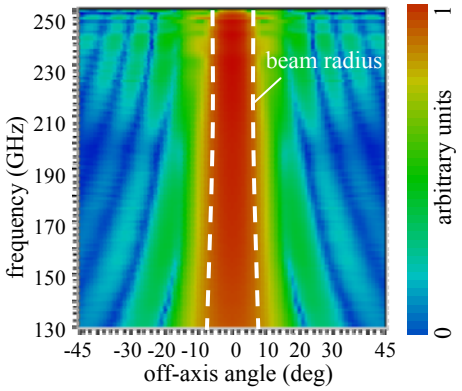

Figure 11. Variation of the re-designed QUBIC horn beam profile (amplitude) as a function of frequency.

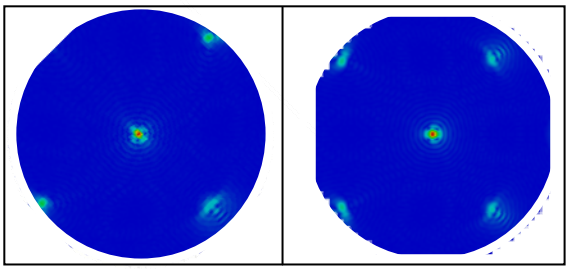

Figure 12. Simulated QUBIC PSF (left) for the 150-GHz module and (right) for the re-designed dual band combiner, operated at 150 GHz.

6. STRAY LIGHT & SHIELDING

For a ground-based instrument a careful analysis of possible contamination from unwanted sources (such as the Sun, Moon and ground) is necessary. Their contribution was calculated using GRASP's multi-GTD technique to find the beam pattern of the central horn (envelope of the synthesised beam) in the presence of the large reflectors of Fig.13. The Sun and Moon were assumed to be at the horizon. For observations at the zenith, for example,

assuming a temperature of 6000 K, 135 K and 300 K for the Sun, Moon and ground, respectively, the spillover contribution was calculated to be 330 μK, 70 μK and 111 mK.

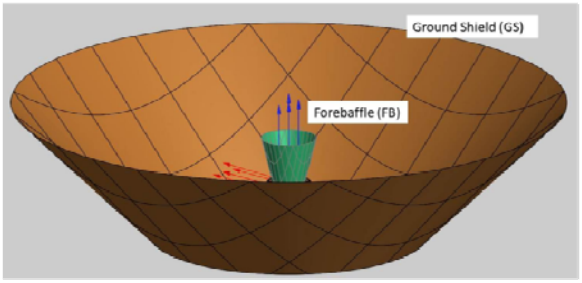

Figure 13. Groundshield and forebaffle tested for QUBIC in preliminary simulations.[22]

Inside the cryostat a straylight analysis using geometric optics has shown that rays emitted at 14° or more can reach the on-axis focal plane directly, and rays emitted at 23° or more can reach the off-axis focal plane. An optical shield around the dichroic will eliminate direct radiation below 16° and reduce radiation at larger angles. This straylight is currently being added to our physical optics model, although we do not expect it to be an issue for QUBIC.

7. SUMMARY

In this paper we have described the design and analysis of the QUBIC optical beam combiner. The requirement for a large aperture and short focal length meant that aberrations we unavoidable. We have shown that the effect of the aberrations present is to reduce the sensitivity of the instrument by 10%, which was considered acceptable.

Recent results from the Planck and BICEP experiments have highlighted the importance of multi-frequency measurements in order to separate polarised foregrounds. It was decided to modify the design of the first QUBIC module so that it will operate at 150 and 220 GHz. We have shown that the optical design can accommodate this change.

8. REFERENCES

1. Planck Collaboration: Ade, P. A. R., et al., (2015). Planck 2015 results. XX. Constraints on inflation. arXiv:1502.02114 [astro-ph.CO].
2. The QUBIC collaboration: Battistelli, E., et al., (2011). QUBIC: The QU bolometric interferometer for cosmology. *Astroparticle Physics* **34**, 705–716.
3. Timbie, P. T., et al., (2006). The Einstein Polarization Interferometer for Cosmology (EPIC) and the Millimeterwave Bolometric Interferometer (MBI). *New Astron. Rev.* **50**, 999-1008.
4. Polenta, G., et al., (2007). The BRAIN CMB polarization experiment. *New Astron. Rev.* **51**, 256–259.
5. Bigot-Sazy, et al., (2013). Self-calibration : an efficient method to control systematic effects in bolometric interferometry. *Astron. & Astrophys.*, **550**, A59.
6. Charlassier, R., et al., (2009). An efficient phase-shifting scheme for bolometric additive interferometry. *Astron. & Astrophys.*, **497**, 963–971.
7. Zemax-EE, ZEMAX Development Corporation. Online at http://www.zemax.com/ (as of August 2015).
8. Rusch W. V. T., et al., (1990). Derivation and application of the equivalent paraboloid for classical offset Cassegrain and Gregorian antennas. *IEEE Trans. Antennas and Propagat.* **38**, (8), 1141.
9. Chang, S., & Prata, Jr., A., (2005). Geometrical theory of aberrations near the axis in classical off-axis reflecting telescopes. *J. Opt. Soc. Am. A*, **22**, (11), 2454-2464.
10. Bennett, D. G., (2014). Design and analysis of a quasi-optical beam combiner for the QUBIC CMB interferometer, PhD Thesis, National University of Ireland, Maynooth.
11. Tran, H., et al., (2008). Comparison of the crossed and the Gregorian Mizuguchi-Dragone for wide-field millimetre-wave astronomy, *Applied Optics* **47**, (2), 103-109, 2008.
12. O'Sullivan, C., et al., (2002). Far Infra-red Optics Design & Verification. *International Journal of Infrared and Millimeter Waves*, **23** (7), 1029-1045.
13. Goldsmith, P.F., (1998). *Quasioptical Systems: Gaussian Beam Quasioptical Propagation and Applications*, IEEE Press series on microwave technology and techniques.
14. Gradziel, M. Ł, et al., (2007). Modelling of the optical performance of millimeter-wave instruments in MODAL, in *Proc. SPIE* 6472, 64720D.
15. GRASP9, TICRA Engineering Consultants. Online at http://www.ticra.dk/ (as of August 2015).
16. Murphy, J. A., et al., (2001). Radiation patterns of multi-moded corrugated horns for far-IR space applications. *Infrared Phys. and Tech.*, **42**, 515-528.
17. Scully, S., PhD Thesis, National University of Ireland, Maynooth (in preparation).
18. Gayer, D., PhD Thesis, National University of Ireland, Maynooth (in preparation).
19. Marie-Anne Bigot-Sazy, M.-A., (2013). PhD Thesis, Université Paris Diderot, Paris 7.
20. BICEP2 Collaboration: Ade, P.A.R., et al., (2014). Detection of B-Mode Polarization at Degree Angular Scales by BICEP2, *Phys. Rev. Lett*. 112, 241101.
21. Taylor, A. C., (2006). Clover - A B-mode polarization experiment. *New Astron. Rev.***50** 993-99.
22. Buzi, D., PhD Thesis, University La Sapienza, Rome (in preparation).